Title

Efficient production of oxidized terpenoids via engineering fusion proteins of terpene synthase and cytochrome P450

Authors

Wang, Xi

Pereira, Jose Henrique

Tsutakawa, Susan

et al.

Publication Date

2021-03-01

DOI

10.1016/j.ymben.2021.01.004

Peer reviewed

Efficient production of oxidized terpenoids via engineering fusion proteins of terpene synthase and cytochrome P450

Xi Wang[1,2], Jose Henrique Pereira[1,3], Susan Tsutakawa[3], Xinyue Fang[1,2,4], Paul D. Adams[1,3,5], Aindrila Mukhopadhyay[1,2], Taek Soon Lee[1,2,*]

[1] Joint BioEnergy Institute (JBEI), 5885 Hollis St., Emeryville, CA 94608, USA

[2] Biological Systems & Engineering Division, Lawrence Berkeley National Laboratory, Berkeley, CA 94720, USA

[3] Molecular Biophysics and Integrated Bioimaging, Lawrence Berkeley National Laboratory, Berkeley, CA 94720, USA

[4] Department of Molecular & Cell Biology, University of California, Berkeley, CA 94720, USA

[5] Department of Bioengineering, University of California, Berkeley, CA 94720, USA.

[*] Corresponding author, Joint Bioenergy Institute, 5885 Hollis Street, Emeryville, CA 94608, USA.

E-mail address: tslee@lbl.gov (T. S. Lee). Tel: +1-510-495-2470. Fax: +1-510-495-2629.

Abstract

The functionalization of terpenes using cytochrome P450 enzymes is a versatile route to the production of useful derivatives that can be further converted to value-added products. Many terpenes are hydrophobic and volatile making their availability as a substrate for P450 enzymes significantly limited during microbial production. In this study, we developed a strategy to improve the accessibility of terpene molecules for the P450 reaction by linking terpene synthase and P450 together. As a model system, fusion proteins of 1,8-cineole synthase (CS) and $P450_{cin}$ were investigated and it showed an improved hydroxylation of the monoterpenoid 1,8-cineole up to 5.4-fold. Structural analysis of the CS-$P450_{cin}$ fusion proteins by SEC-SAXS indicated a dimer formation with preferred orientations of the active sites of the two domains. We also applied the enzyme fusion strategy to the oxidation of a sesquiterpene epi-isozizaene and the fusion enzymes significantly improved albaflavenol production in engineered *E. coli*. From the analysis of positive and negative examples of the fusion strategy, we proposed key factors in structure-based prediction and evaluation of fusion enzymes. Developing fusion enzymes for terpene synthase and P450 presents an efficient strategy toward oxidation of hydrophobic terpene compounds. This strategy could be widely applicable to improve the biosynthetic titer of the functionalized products from hydrophobic terpene intermediates.

Keywords

Oxidized terpenoid, fusion protein, terpene synthase, P450, SAXS, I-TASSER

1. Introduction

Terpenes are a large class of natural products, primarily produced by plants and constitute the main components of essential oils. A typical monoterpene (C_{10}), such as limonene, is a cyclic hydrocarbon molecule ($C_{10}H_{16}$) and can be used as a precursor of fuel additives, fragrances, insecticides, and pharmaceuticals (Aharoni et al., 2005). Production of terpenes in the microbial system is considered a more sustainable and stable alternative to the isolation from plants or via chemical synthesis. Functionalization of the terpene carbon backbone by enzymes such as cytochrome P450s could further expand the range of bio-based compounds which frequently can be converted to additional products of commercial interest (Bernhardt, 2006; Chang et al., 2007; Pateraki et al., 2015; Renault et al., 2014; Urlacher and Girhard, 2019). For example, limonene can be oxidized by P450 (CYP153) to perillyl alcohol, a precursor of promising anti-cancer agents (van Beilen et al., 2005). While P450s play an important role in the decoration and modification of terpenes essential for the new bioactivities, the hydrophobicity and volatility of terpene molecules might limit the availability of the substrate around the enzyme and result in low enzymatic conversion during microbial production, especially when a solvent overlay is used to reduce the loss of these volatile compounds via extraction of hydrophobic terpenes to the overlay (Alonso-Gutierrez et al., 2013). This makes the subsequent enzymatic reaction (which uses terpenes as substrates) less efficient and eventually lowers the titer of the final product.

To overcome the low availability of hydrophobic substrates for downstream enzymes such as P450s, one popular strategy is to create a spatial constraint that improves the proximity between the enzyme and the substrate (Conrado et al., 2008). Engineering of fusion proteins (Kourtz et al., 2005; Meynial Salles et al., 2007), protein scaffolds (Dueber et al., 2009), and compartmentalization of metabolic pathways (Avalos et al., 2013) have been explored to achieve

the proximity effect. Among these approaches, engineering synthetic fusion proteins have been extensively used to modify enzymes toward efficient metabolic catalysis due to their simplicity and effectiveness (Yu et al., 2015). Using a short peptide linker sequence, two or more enzymes are combined and generate a single polypeptide that exhibits more than one activity or increases the reaction rate for consecutive enzymes. In the microbial production of isoprenoids, a higher pinene production level was reported by linking terpene synthase with geranyl pyrophosphate (GPP) synthase to overcome product inhibition from GPP (Sarria et al., 2014). Similarly, an engineered fusion of isopentenyl diphosphate (IPP) isomerase and isoprene synthase showed a 3.3-fold increase of isoprene titer (Gao et al., 2016). For P450 enzymes, fusions of P450 with a heterologous cytochrome P450 reductase have also proven successful in various instances. For example, a P450 TxtE was linked to the reductase domain of P450BM3 for improved activity and regio-promiscuity in aromatic nitration (Zuo et al., 2017).

Although engineering a fusion of P450 with a cytochrome P450 reductase is widely studied, there are fewer reports for engineering a fusion between P450 and a terpene synthase. Given that the considerable loss of the terpene substrate from the cell is a critical limitation for the subsequent P450 reaction during the microbial production (Alonso-Gutierrez et al., 2013), engineering a fusion protein by linking terpene synthase and P450 to form a chimeric protein could improve the proximity of P450 and the terpene substrate, which in turn would improve the substrate availability for P450. In this study, we selected the hydroxylation of monoterpene 1,8-cineole as a model system to demonstrate this approach in the microbial system via engineering the recombinant enzyme fusion between terpene synthase-P450 enzyme fusion (Figure 1). Guided by structural modeling, we engineered a series of fusion proteins between 1,8-cineole synthase and $P450_{cin}$ (CYP176A1) to investigate the hydroxylation of 1,8-cineole in both *in vitro*

and *in vivo* conditions in comparison to non-fused enzymes. Structural analysis of fusion proteins revealed that different linker length changes the flexibility of the fusion enzymes. We also applied this enzyme fusion strategy for the oxidation of several other terpenes, and the data from both experiments and the modeling analysis, of positive and negative results suggested key factors (e.g. linker length, enzyme orientation, etc.) for designing a fusion protein. Our results demonstrated that engineering fusion enzyme is a feasible strategy for the efficient production of functionalized products from hydrophobic terpene intermediates.

2. Material and methods

2.1 Strains and plasmid construction

All strains and plasmids used in this study are listed in Table 1. Strains and plasmids along with their associated information have been deposited in the public domain of the JBEI Registry (https://public-registry.jbei.org; entries JPUB_016968 to JPUB_017025) and are available from the authors upon request. *E. coli* DH1 strain was used for terpene and oxidized terpene production, and *E. coli* DH5α was used for genetic cloning. Genes of CinA ($P450_{cin}$, CYP176A1; GenBank ID: AF456128) and CinC (Cindoxin, Cdx, GenBank ID: AF456128) from *Citrobacter braakii*, and CYP170A1 (*sco5223*; GenBank ID: NC_003888) from *Streptomyces coelicolor* A3(2) were codon-optimized and synthesized by Integrated DNA Technologies, Inc. (San Diego, CA, USA). Fpr (GenBank ID: CP032667) was cloned from *E. coli* genomic DNA. CS from *Streptomyces clavuligerus* was cloned from plasmid JBEI-15065 (Table 1). All peptide linkers were introduced onto the plasmid by PCR using primers listed in Supplementary Table S1.

2.2 Protein expression and purification

A plasmid pSKB3 encoding interested proteins with N-terminal His-tag was transformed into *E. coli* BL21 (DE3). BL21 (DE3) strains bearing pSKB3 plasmids were cultured in Lysogeny Broth (LB) medium containing 50 μg/mL kanamycin at 37°C until the optical density of the culture at 600 nm (OD_{600}) reached to 0.5 – 0.8. The culture was then supplemented with 0.4 mM isopropyl β-D-1-thiogalactopyranoside (IPTG) for induction and transferred to 18°C for culturing overnight. Cells were collected by centrifugation and resuspended in 25 mM Tris-HCl (pH 8.0) buffer containing 300 mM NaCl and 10 mM imidazole (pH 8.0). Cells were lysed by sonication and proteins were purified using Ni-NTA Agarose (QIAGEN, Hilden, Germany). All purified proteins were desalted in 25 mM Tris-HCl (pH 8.0) buffer containing 100 mM NaCl, and 10% glycerol, and stored at -80°C. A Bradford assay (Sigma-Aldrich, St. Louis, MO, USA) was used to quantify the protein concentration of purified proteins, with bovine serum albumin (BSA) as a standard. The quantification of $P450_{cin}$ was determined by UV absorption at 415 nm (ε = 150 $cm^{-1}mM^{-1}$) (Slessor et al., 2012), and for redox proteins: Cdx at 456 nm (ε = 10825 $cm^{-1}M^{-1}$) (Hawkes et al., 2010), Fpr at 456 nm (ε = 7100 $cm^{-1}M^{-1}$) (Jenkins and Waterman, 1994). Both quantification results were shown in the Supplementary Table S4.

2.3 *In vitro* production of hydroxycineole

Using purified proteins, Bradford-quantified non-fusion (5 μM CS + 5 μM CinA) or fusion proteins (5 μM) were used for the *in vitro* production of hydroxycineole with 40 μM CinC and 10 μM Fpr in 50 mM Tris-HCl buffer (pH 7.4) containing 5 mM $MgCl_2$ (Hawkes et al., 2010; Shaw et al., 2015). NADPH (2 mM) and 1 mM geranyl pyrophosphate (GPP, Sigma-Aldrich

19533) were added to start the reaction. The reaction was conducted in a total volume of 600 µL reaction in a 1.7-mL microcentrifuge tube at 25°C for 5 hours.

2.4 *In vivo* production of hydroxycineole

E. coli DH1 bearing two plasmids (JBEI-3122 + JPUB_016986 to JPUB_010998, Table 1) was used for hydroxycineole production. Starter cultures of all production strains were prepared by growing single colonies in LB medium containing 30 µg/mL chloramphenicol and 100 µg/mL carbenicillin at 37°C with 200-rpm shaking for overnight. The starter cultures were diluted in 5 mL EZ-Rich defined medium (Teknova, CA, USA) containing 10 g/L glucose (1%, w/v), 30 µg/mL chloramphenicol, 100 µg/mL carbenicillin, and 0.5 mM IPTG in 50-mL test tubes. 0.5 mL nonane (10%, v/v) was added when required as a solvent overlay. The *E. coli* cultures were incubated in rotary shakers (200 rpm) at 30°C for 48 hours.

2.5 *In vivo* production of oxidized epi-isozizaene

E. coli DH1 bearing two plasmids (JBEI-2704 + JPUB_017000 to JPUB_017009, Table 1) was used for oxidized epi-isozizaene production. Starter cultures of all production strains were prepared by growing single colonies in LB medium containing 30 µg/mL chloramphenicol and 100 µg/mL carbenicillin at 37°C with 200-rpm shaking for overnight. The starter cultures were diluted in 5 mL EZ-Rich defined medium (Teknova, CA, USA) containing 10 g/L glucose (1%, w/v), 30 µg/mL chloramphenicol, 100 µg/mL carbenicillin, and 65 mg/L δ-aminolevulinic acid, 0.5 mM IPTG in 50-mL culture tubes. 0.5 mL nonane (10%, v/v) was added when required as a solvent overlay. The *E. coli* cultures were incubated in rotary shakers (200 rpm) at 30°C for 72 hours.

2.6 Protein structure prediction

Structures of fusion proteins were predicted by Iterative Threading ASSEmbly Refinement (I-TASSER) server (Roy et al., 2012; Yang and Zhang, 2015; Zhang, 2009). The predicted models with the highest C-score were used for further analysis. For the non-fusion enzyme CS (PDB: 5NX6) (Karuppiah et al., 2017), $P450_{cin}$ (PDB: 1T2B) (Meharenna et al., 2004), EizS (PDB: 3KB9) (Aaron et al., 2010), CYP170A1 (PDB: 3DBG) (Zhao et al., 2009), LS (PDB: 2ONG) (Hyatt et al., 2007), and CYP153A6 (similar sequence to CYP153A7, PDB: 3RWL) (Pham et al., 2012), their structural models or homology model were retrieved from PDB and aligned with the predicted structures of correlated fusion proteins. Active sites of subunits in the fusion proteins were annotated according to literature. PyMOL was used for visualization and image generation.

2.7 Small Angle X-ray Scattering (SAXS)

Size Exclusion Chromatography (SEC) coupled to Small Angle X-ray Scattering **(**SAXS) data were collected at the beamline 12.3.1 at the Advanced Light Source synchrotron (Lawrence Berkeley National Laboratory, Berkeley, CA, USA) (Classen et al., 2013). Proteins were separated on an SEC Shodex KW-803 column at 20°C in 25 mM Tris HCl, pH 7.5, 50 mM NaCl and eluted directly into the SAXS sample cell at a flow rate of 0.5 mL/min. Three second X-ray exposures were collected continuously over the 30 minutes SEC elution at 1.127Å wavelength on a Dectris PILATUS3 × 2M detector. Initial data were processed at the beamline (Dyer et al., 2014; Hura et al., 2009). The sample to detector distance was 2.105 m. The SAXS eluent was split 4 to 1 between the SAXS sample cell and UV, multi-angle light scattering (MALS), and refractometer, measured on an 18-angle DAWN HELEOS II light scattering detector and Optilab

refractive index concentration detector (Wyatt Technology, CA, USA). The system was calibrated with bovine serum albumin (BSA). Background subtraction from SAXS frames after the protein peaks and evolving factor analysis (EFA) was done using the program RAW. Representing tetrameric, dimeric, and monomeric population, three components were derived from the peak eluting at ~20 minutes. SAXS frames after the main peak were used for buffer subtraction. The targeted elution peak was deconvoluted into three components, representing monomer, dimer, and tetramer. Further SAXS analysis was done using RAW (Volume of Correlation MW) (Rambo and Tainer, 2013), SCÅTTER (Porod component, https://bl1231.als.lbl.gov/scatter/), ATSAS (Guinier, Real space, GASBOR) (Franke et al., 2017). In the Guinier plots, all SAXS curves were linear, consistent with no aggregation present. Based on the crystal structures of the subunits (PDB: 5NX6 and 1T2B), SAXS models were built using MODELER (Fiser et al., 2000), followed by BilBOMD/FOXS (Pelikan et al., 2009; Schneidman-Duhovny et al., 2016, 2013). SAXS data collection and data analysis details are provided in Table 2.

2.8 Gas chromatography-mass spectrometry (GC-MS) analysis

For 1,8-cineole, hydroxycineole, and perillyl alcohol, samples were extracted by an equal volume of ethyl acetate containing β-pinene (5 mg/L) as an internal standard. For epi-isozizaene and oxidized products, samples were extracted by an equal volume of ethyl acetate containing guaiazulene (5 mg/L) as an internal standard. The mixture of ethyl acetate and *in vitro* reaction solution or cell culture was vigorously shaken for 15 min and subsequently centrifuged at 21,130 g for 3 min to separate ethyl acetate from the aqueous phase. The ethyl acetate layer was collected and 1 µL was analyzed by Agilent GC-MS equipped with HP-5 column (Agilent,

USA). The GC oven was programmed from 40°C (held for 3 min) to 295°C at 15°C/min. The solvent delay was set at 3.4 min. 1,8-cineole and perillyl alcohol were quantified using authentic standards. Hydroxycineole concentration was estimated using total ion chromatogram (TIC) areas with respect to the TIC areas of alternative standard 1,8-cineole, and β-pinene (a monoterpene) as an internal standard to normalize the GC results. Similarly, the concentrations of epi-isozizaene, albaflavenol, and albaflavenone were estimated using their TIC areas with respect to the TIC areas of alternative standard (-)-trans-caryophyllene, and guaiazulene (a sesquiterpene) was used as an internal standard to normalize the GC results. MS full scan spectrum of hydroxycineole and oxidized epi-isozizaene were shown in Supplementary Figures S1 and S2. When nonane overlay was used during the production, the solvent delay was set at 6.8 min. Both the nonane overlay and the aqueous phase of the culture were sampled for the GC-MS measurement, respectively. The production titers were the sum of both measured values after applying the dilution factor.

3. Results

3.1 Designing fusion enzymes of 1,8-cineole synthase and $P450_{cin}$

1,8-Cineole, or eucalyptol, is a monoterpene (C10) naturally found in essential oils from *Eucalyptus globulus* and other plants. (Klocke et al., 1987; Shaw et al., 2015). 1,8-Cineole is also a potential precursor for high energy-density molecules used as jet fuels (Bergman and Siewers, 2016; Yang et al., 2017), and therefore *E. coli* was engineered previously to overproduce 1,8-cineole using the mevalonate (MVA) pathway (Mendez-Perez et al., 2017). Hydroxylation of 1,8-cineole introduces a functional group to this compound and allows further derivatization to more valuable products, such as *p*-cymene (Leita et al., 2010). $P450_{cin}$ (CYP176A1) from *C.*

braakii has shown a specific activity of 1,8-cineole hydroxylation to produce (1*R*)-6β-hydroxycineole (or hydroxycineole) (Hawkes et al., 2002), and its redox partners, NADPH-dependent flavodoxin reductase and a flavodoxin, have also been reported (Hawkes et al., 2010).

To investigate the hydroxylation of 1,8-cineole as a model system for engineering the enzyme fusion between terpene synthase and P450, fusion proteins were designed between 1,8-cineole synthase (CS) and $P450_{cin}$ using a flexible peptide linker Gly-Ser-Gly (GSG) (Guo et al., 2017). First, we have predicted the structure of CS-$P450_{cin}$ fusion proteins linked by $(GSG)_n$ linkers using the I-TASSER server (Roy et al., 2012; Yang and Zhang, 2015; Zhang, 2009). The modeling provided a possible orientation of the CS and $P450_{cin}$ fusion proteins (Figure 2), and the results showed that the two active sites of CS and $P450_{cin}$ were proximally oriented. Based on the preliminary structural analysis of CS-$P450_{cin}$ fusion proteins, we engineered five CS-$P450_{cin}$ fusion proteins with different linker lengths by adjusting the repeat number (n) of $(GSG)_n$ linker (n = 1–5), and the resultant CS-$P450_{cin}$ fusion proteins were named G1 to G5, respectively according to their number of GSG linker repeats.

3.2 *In vitro* production of hydroxycineole with CS-$P450_{cin}$ fusions from GPP

To investigate the hydroxylation of 1,8-cineole by various CS-$P450_{cin}$ fusions with different linker lengths, equal moles of purified proteins were used for *in vitro* production of hydroxycineole from GPP substrate (Figure 3). In a 5-hour reaction, most CS-$P450_{cin}$ fusions except G1 showed a higher level of hydroxycineole production than non-fused individual CS and $P450_{cin}$. The G1 fusion did not show a substantial difference relative to the non-fusion control (Figure 3C). The highest level of hydroxycineole production was observed from the G4 fusion and showed a 5.4-fold increase over non-fused CS and $P450_{cin}$ after 5 hours. The highest

hydroxycineole production rate in G4 was reached after 2 hours at 0.051 μM/min, which is 6.4-fold faster than that of the non-fusion enzymes (0.008 μM/min). The overall hydroxylation ratio of the G4 fusion was 2.3% after 5 hours, which is 5.4-fold higher than that of the non-fusion enzymes (0.4%) (Figure 3D). All 5 fusion enzymes also showed up to a 2.7-fold increase of 1,8-cineole level over the non-fused enzymes during the first 3 hours (Figure 3C), suggesting that enzyme fusion also improves the activity of the cineole synthase and eventually more terpene substrate is available for the P450 reaction with the fusion proteins. Likely due to the volatility of 1,8-cineole, it was also observed that 1,8-cineole eventually decreased to a similar level from all different samples after a 3-hour reaction (Figure 3C).

The *in vitro* production results with the engineered CS-$P450_{cin}$ fusions showed higher hydroxycineole production than non-fused CS and $P450_{cin}$. The improved 1,8-cineole hydroxylation from fusion proteins could be attributed to the proximity of $P450_{cin}$ to its hydrophobic substrate 1,8-cineole, which shows the advantage of linking a P450 enzyme to a terpene synthase, particularly when a hydrophobic and volatile terpene is the intermediate and served as the substrate for a consequential P450 reaction during a multi-step terpene oxidation.

3.3 *In vivo* assessment of CS-$P450_{cin}$ fusions for hydroxycineole production from glucose

To *in vivo* assess hydroxycineole production using fusion enzymes, the CS-$P450_{cin}$ fusions were introduced into *E. coli*. Informed from the previous report (Mendez-Perez et al., 2017), *E. coli* strain containing 2 separate plasmids was used for hydroxycineole production by inserting the genes encoding the $P450_{cin}$ (CinA) and its redox partner Cdx (CinC) downstream of CS on the 2nd plasmid JBEI-15065 (Table 1). For the expression of the non-fused CS and $P450_{cin}$, an RBS sequence (5'-TTTAAGAAGGAGATATAC-3') was used for individual expression of CS

and $P450_{cin}$, respectively (Table 1 and Supplementary Table S1). For the CS-$P450_{cin}$ fusions, the same RBS was used for the entire fused gene sequence. As solvent overlay is usually used to prevent evaporation of the product during production, we used the overlay to evaluate the performance of fusion enzymes at the *in vivo* conditions. While dodecane was used as the overlay for 1,8-cineole production previously (Mendez-Perez et al., 2017), it has a similar molecular weight to hydroxycineole (MW=170), as well as a close retention time in chromatography. Therefore, we used nonane instead of dodecane as the overlay to obtain a better signal of hydroxycineole by GC-MS.

As shown in Figure 4, the use of solvent overlay generally facilitated 1,8-cineole production, but it did not help hydroxycineole levels. For both non-fusion and fusion proteins, hydroxycineole production without using overlay was 1.7 to 3.3-fold higher than that with an overlay. When nonane overlay was used, all fusions except G4 detected more hydroxycineole than the non-fusion control strain (Figure 4C), while generally less amount of 1,8-cineole (except for G2), suggesting an inefficient hydroxylation in the non-fusion control strain. When overlay was not used during the production, all 5 strains with fusion protein produced more hydroxycineole than the non-fusion control strain (Figure 4C). The highest hydroxycineole titer was observed from G3 (56 mg/L), which is 3.1-fold higher than that of the non-fusion control (18 mg/L). In contrast to the *in vitro* results, G4 did not show any significant advantage compared with the other fusions with different linker lengths. Similar to our previous work of a P450 conversion perillyl alcohol from limonene (Alonso-Gutierrez et al., 2013), the addition of solvent overlay facilitated the *in situ* extraction of 1,8-cineole and prevents the evaporation from the culture, but it also competed with the subsequent P450 enzymatic reaction for terpene substrates and eventually lower the P450 bioconversion efficiency. Overall, the use of fusion

proteins improved the production of hydroxycineole with and without added solvent overlay, which suggested a higher efficiency during *in vivo* production of the oxidized terpene.

In addition to the linker length, the enzyme orientation is another key factor for the activity of a fusion enzyme (Sarria et al., 2014). Given that G3 showed high production of hydroxycineole both *in vitro* and *in vivo* conditions, we used the $(GSG)_3$ linker to construct a fusion enzyme $P450_{cin}$-$(GSG)_3$-CS by switching the order of CS and $P450_{cin}$ and to test hydroxycineole production. Compared to the CS-$(GSG)_3$-$P450_{cin}$ fusion (G3), this fusion enzyme with reversed domain order produced 51% and 76% less 1,8-cineole and hydroxycineole, respectively when the overlay was used (Table 3). These trends were also significant when the overlay was not used. In this case, it produced 80% and 63% less 1,8-cineole and hydroxycineole, respectively, than in the G3 fusion protein (Table 3), indicating the inefficiency when CS and $P450_{cin}$ were linked in the reversed orientation. This $P450_{cin}$-$(GSG)_3$-CS fusion enzyme did not even result in a significant improvement of hydroxycineole but less 1,8-cineole production compared with the non-fusion control strain (Table 3). Structural modeling results suggested that the two active sites of $P450_{cin}$ and CS in this fusion protein are no longer proximally oriented (Supplementary Figure S3). As shown in Figure S3A, the active site of CS faces outside of the fusion complex surface, whereas the active site of $P450_{cin}$ is located in the middle of the fusion complex. Thus, the simulated fusion structure shows an unfavorable orientation for the two subunits and may explain its less efficiency as a fusion protein.

3.4 Structural characterization of CS-$P450_{cin}$ enzyme fusions

To experimentally determine the orientation of CS and $P450_{cin}$, we used Size Exclusion Chromatography coupled to Small Angle X-ray Scattering (SEC-SAXS) to characterize the G3

and G4 fusion proteins in solution as these two fusion enzymes showed the best activities at the *in vitro* experiments. SAXS measures electron pair distances of proteins in solution and can reveal protein stoichiometry, flexibility, and overall orientation, in cases such as ours where the individual subunits have been crystallized (Putnam et al., 2007). For both G3 and G4 fusion proteins in the size exclusion chromatography profile, the proteins eluted in multiple peaks, with the earliest peak representing large aggregates and the second major peak representing a mixture of monomer, dimer, and tetramer, based on SAXS molecular mass calculation and in agreement with in-line Multi-Angle Light Scattering (MALS) measurements (Figure 5A).

For the G3 fusion protein, the aggregate peak was higher in the UV signal than the monomer/dimer peak, but the second peak was larger than the aggregate peak in the G4 fusion protein (Figure 5A). The different proportions of peaks suggested that the G3 fusion protein may be more constrained than the G4 fusion protein. The SAXS frames from the second peaks were deconvoluted into three SAXS components, representing monomer, dimer, and tetramer. For both G3 and G4 fusion proteins, the dimer population was greater than monomer or tetramer, based on MALS and relative intensity of the scattering profile, even taking into account the greater scattering of the dimer compared to the monomer. A measure of the protein density and relative flexibility, the Porod Debye number for the G4 monomer and dimer were both 3.3 (Table 2), consistent with the protein behaving like beads on a string (Brosey et al., 2013; Rambo and Tainer, 2011). The number for the G3 monomer and dimer were 3.9 and 3.4 (Table 2), respectively, indicating greater rigidity in the G3 fusion protein.

Using two different modeling programs followed by molecular dynamics, we generated models of the G3 and G4 monomer and dimer to match against the experimental SAXS data (Figure 5B and 5C). The analysis compares single models and ensembles of models, the latter of

which are usually found to best fit experimental SAXS data when there is significant flexibility. Surprisingly, we found that the experimental SAXS data curves fit well against single models, despite the flexibility indicated by the Porod Debye number in three of the SAXS curves. This SAXS modeling result suggests the two domains of CS and $P450_{cin}$ are shifting relative to each other but not completely swinging free (Figure 5D). For the monomer of fusion proteins, the SAXS structural analysis matched the predicted structure by I-TASSER for the fusion protein sequence (Figure 2), and the formalized dimers of fusion protein could also intensify the proximity effect.

3.5 Production of oxidized epi-isozizaene using enzyme fusions.

We applied the enzyme fusion strategy to the biosynthetic pathway for oxidized epi-isozizaene products (Figure 1, Figure 6) such as albaflavenol, and the subsequently oxidized product albaflavenone, a sesquiterpene antibiotic found in *S. coelicolor* A3(2) (Zhao et al., 2008). A bacterial P450 (CYP170A1) has been identified to catalyze the oxidation of epi-isozizaene in *S. coelicolor* A3(2). Recently, epi-isozizaene biosynthesis was successfully engineered in *E. coli* to produce a novel jet-fuel precursor using the MVA pathway (Liu et al., 2018). To build the fusion protein for epi-isozizaene synthase (EizS) and CYP170A1, we predicted the possible structure of an EizS-CYP170A1 fusion protein, and it showed the proximal orientation for the two active sites of EizS and CYP170A1 in the fusion (Supplementary Figure S4). Following the fusion enzyme engineering strategy used in hydroxycineole biosynthesis, we constructed fusions for EizS and CYP170A1 with 1 to 5 repeats of Gly-Ser-Gly (GSG) peptide linker. An RBS sequence (5'- TTTCACACAGGAAACAGACC-3') was used for the expression of EizS and CYP170A1 individually in the non-fusion control

strain similar to the 1,8-cineole oxidation case. For the EizS-CYP170A1 fusions, the same RBS was used for the entire fused gene sequence (Table 1, Supplementary Table S1).

Compared with the non-fusion control, the epi-isozizaene production level was a little lower in the strains engineered with fusion enzymes (Figure 6C). On the other hand, the total oxidized products (albaflavenol and albaflavonone) were notably increased in the fusions with shorter linkers $(GSG)_{1-3}$ for both conditions, with and without added solvent overlay (Figure 6D). As expected, the improvement of oxidized products by enzyme fusions was more significant when the overlay was used. The highest oxidized epi-isozizaene level (13 mg/L albaflavenol, 3 mg/L albaflavenone) was observed by the fusion EizS-$(GSG)_2$-CYP170A1 with a $(GSG)_2$ linker, which achieved 90- and 2.3-fold increase in albaflavenol and albaflavenone production, respectively. This result demonstrated the viability of engineering a fusion protein between terpene synthase and P450 for sesquiterpene oxidation, suggesting possible applications of this enzyme fusion strategy to functionalize diverse terpenoid compounds.

4. Discussion

In this study, we used an enzyme fusion strategy by directly linking terpene synthase and cytochrome P450 to facilitate the heterologous production of oxidized terpenoids in engineered microbial systems. Unlike the natural biosynthesis process in plants (Cheng et al., 2007; Pateraki et al., 2015), engineered microbial systems usually lack cellular compartments and spatial regulation to contain the volatile molecules. By taking advantage of the proximal environment created by the fusion enzyme, we expected the fusion can facilitate the capture of volatile terpene molecules for downstream P450s and improve the terpene oxidation. Using the monoterpene 1,8-cineole hydroxylation as a model system, fusion proteins of 1,8-cineole synthase (CS) and

386 $P450_{cin}$ (CYP176A1) were constructed with different lengths of peptide linkers. The engineered
387 CS-$P450_{cin}$ fusions showed improved hydroxylation of 1,8-cineole at both *in vitro* and *in vivo*
388 conditions. During the *in vitro* hydroxycineole production, all CS-$P450_{cin}$ fusions showed a faster
389 accumulation of 1,8-cineole than the non-fused individual enzyme case (Figure 3C). This might
390 be a result from a reduced loss of 1,8-cineole in the proximal environment created by the fusion
391 enzyme that facilitates the capture of 1,8-cineole and reduces the diffusion loss in solution. The
392 increased availability of the terpene substrate could be a key factor that leads to higher
393 production rates observed for $P450_{cin}$ in fusion proteins (Supplementary Table S3), which
394 indicated that the non-fused $P450_{cin}$ could remain in a suboptimal activity in a two-step terpene
395 oxidation. As many terpenes are usually hydrophobic and volatile compounds, the availability of
396 terpene substrates is critical to reaching the maximum activity for a consequent P450 enzyme in
397 the multi-step enzymatic oxidation of terpenoids. Additionally, the nature of CS dimerization
398 (Karuppiah et al., 2017) could play an important role in enhancing the entire activity of a CS-
399 $P450_{cin}$ fusion protein. Similar results were reported in a fusion of *E. coli* beta-galactosidase
400 (LacZ) and the dimeric galactose dehydrogenase (GalDH) from *Pseudomonas fluorescens*,
401 which showed improved enzyme activities when they are linked to each other (Ljungcrantz et al.,
402 1989).
403 While spatial proximity explains the most advantages of a fusion protein relative to the
404 corresponding non-fused enzymes, we observed fusion proteins with different linker lengths
405 showed distinct activities. Surprisingly, the best fusion protein (G4) with 4-repeats of Gly-Ser-
406 Gly linker from the *in vitro* conditions did not show the best production level under the *in vivo*
407 conditions (Figure 3C, Figure 4C). This indicated that the optimal linker length for a fusion
408 protein may vary from the *in vitro* and *in vivo* conditions because of their inconsistent reaction

409 conditions, such as the ratio of $P450_{cin}$ and redox partners. This may also suggest that an optimal
410 linker length plays a key role in selecting the best activity of a fusion enzyme. Similar
411 observations have also been reported previously. For example, a fusion of *Marinobacter*
412 *aquaeolei* P450 (CYP153) and a CYP116B reductase showed 67% improvement of activity by
413 adding two extra amino acids in the linker (Hoffmann et al., 2016), and in another example, a ten
414 amino-acid linker was found to present the best activity in the fusion of $P450_{cin}$ with its native
415 flavodoxin (CinC) (Belsare et al., 2014).

416 To experimentally reveal the difference caused by the linker length, we pursued the structural
417 analysis for G3 and G4 fusions which are selected with the best activities at the *in vitro*
418 conditions. The SEC-SAXS data and modeling results suggested they showed different structural
419 rigidities for the G4 fusion protein with a 12-aa linker and is less constrained, relative to the G3
420 fusion containing a 9-aa linker (Table 2, Figure 5D). This difference brought by the linker length
421 indicated its importance in maintaining the rigidity of a fusion complex as well as reaching the
422 best activity of a fusion protein. In addition to the linker length, the different ratios of P450 and
423 redox partners could change the P450 conversion in a wide range (Hawkes et al., 2010; Khatri et
424 al., 2017). Therefore, precision modulation of the *in vivo* P450-redox ratio presents a promising
425 strategy to improve the P450 conversion yield for microbial production systems (Li et al., 2020;
426 Schiffer et al., 2015).

427 Besides, the orientation of active sites in a fusion protein is another critical factor to achieve
428 improved catalysis over the non-fused enzymes. In the assessment of the enzyme orientation in a
429 fusion protein, we found reversing the order of CS and $P450_{cin}$ in the fusion protein dramatically
430 decreased the catalytic efficiency (Table 3), and even did not show significant improvement of
431 the activity over the non-fusion control. Given that the key interface residues R102 and R346

(Madrona et al., 2014) of $P450_{cin}$ for the constitution of $P450_{cin}$-Cdx were intact for both CS-$P450_{cin}$ and $P450_{cin}$-CS fusions (Supplementary Figure S3), we think this inefficient fusion construction might be more likely attributed to their relative position of the active sites in two domains. As the structural modeling predicted, the two active sites of CS and $P450_{cin}$ showed an unfavorable orientation in the $P450_{cin}$-CS fusion protein, which may increase the difficulty for 1,8-cineole to access the binding sites of $P450_{cin}$ (Supplementary Figure S3). We also observed similar results in another negative example that implemented the enzyme fusion strategy in perillyl alcohol production by the hydroxylation of limonene (Supplementary Information). In this case, structural modeling predicted unfavorable orientation of two active sites for limonene synthase (LS) and CYP153A6 in the built fusion protein (Supplementary Figure S5B), and the experimental results also did not show any improvement in perillyl alcohol production in five fusion proteins engineered with different linker lengths (Supplementary Figure S5C).

The SAXS structural analysis suggested that the linker length can change the structural flexibility of domains in a fusion protein, but it may not easily change the orientation of enzyme active sites in a fusion complex due to the associated rigidity. Thus, for those fusion proteins showing an unfavorable orientation between two active sites, the loop structure at the terminus of the first enzyme might be a key to overcome the native rigidity of two domains and to facilitate the favorable orientations in the fusion. In a comparison of positive and negative examples we studied, we observed that each of two negative examples (LS-CYP153A6 and $P450_{cin}$-CS fusions) shows a relatively short C-terminal loop of the first enzyme (i.e. LS has a 4-aa loop and $P450_{cin}$ has a 7-aa loop), while the first enzymes of positive examples (CS-$P450_{cin}$ and EizS-CYP170A1 fusions) have long C-terminal loops (i.e. CS has a 19-aa loop and EizS has a 21-aa

loop) (Supplementary Figure S6). Therefore, the engineering of terminal loops could be a potential target to design fusion protein more adequately.

While engineering of fusion proteins shows a feasible approach for desirable enzymatic characteristics, it is still challenging to achieve the optimal activities. For example, it is difficult to precisely control the distance or orientation of enzymatic modules in a fusion protein. Also, the correct folding of a large multidomain protein could be difficult. Many P450 enzymes from plants are membrane-bound and have shown poor soluble expression in the bacterial hosts such as *E. coli* (Moser and Pichler, 2019). Thus, more consideration would be needed when engineering a fusion for eukaryotic terpene synthases and the membrane bound P450s in heterologous hosts. For example, truncating plastidial targeting sequence was found to improve the heterologous expression and catalytic efficiency of (4*S*)-limonene synthase from *Mentha spicata* (spearmint) in *E. coli* (Hyatt et al., 2007; Williams et al., 1998). Also, modifying N-terminal sequences of cytochrome P450 (CYP71D18, *M. spicata*) increased P450 expression as well as limonene hydroxylation rate in *E. coli* and yeast (Haudenschild et al., 2000).

The successful construction of a fusion enzyme relies on many factors, including domain order, inter-domain distance, domain orientation, and linker properties (Yu et al., 2015). Although several modeling programs have been reported to facilitate the designing of linkers for fusion protein engineering (Crasto and Feng, 2000; Liu et al., 2015), an in-depth structural analysis could be more important to design the optimal linker and the enzyme orientations to build an enzyme fusion with improved catalysis. Based on our experimental results and structural modeling analysis for fusion enzymes with both positive and negative results, we found the key factors in designing an efficient fusion protein include linker length, enzyme orientation, and potentially the terminal loops of each domain. Therefore, the combination of these factors guided

by structural modeling would be an effective strategy to design and optimize the activity of a fusion enzyme.

The efficiency of the P450 bioconversion of terpenoids to oxidized products observed in our studies is still low for both non-fusion and fusion proteins. This low efficiency could be a result of the relatively low percentage of active P450 as observed in the $P450_{cin}$ example (Supplementary Table S4). Interestingly, it is noted that the engineered fusion proteins could affect the functional expression of the active portion of $P450_{cin}$. Compared with the non-fusion $P450_{cin}$, some fusions (G2-G5) showed a lower percentage of the active $P450_{cin}$ portion despite higher productivities for hydroxycineole while other fusion (G1) showed a higher percentage of the active portion with lower productivity. Further optimization of the P450 enzymes and the *in vivo* microbial production system is necessary to improve the conversion yield, such as increasing the active P450 portion, identifying more efficient redox partners and the ratio of P450 and redox partners (Hawkes et al., 2010; Kimmich et al., 2007), engineering fusions of redox partners for enhanced electron transfer (Bakkes et al., 2017, 2015), optimizing the metabolic pathway for terpene substrate overproduction and co-factor balance, developing *in situ* extraction reagent (e.g. resins) to facilitate the collection of oxidized products (Alonso-Gutierrez et al., 2013).

5. Conclusions

The functionalization of terpene molecules using cytochrome P450 enzymes presents opportunities to produce various bioproducts that are frequently more value-added than the original terpene itself. In this study, we developed a strategy to improve the terpene hydroxylation efficiency by linking terpene synthase and P450 enzyme and facilitating the accessibility of terpene molecules to P450 enzymes in heterologous microbial systems. We

demonstrated this strategy for monoterpene 1,8-cineole hydroxylation and achieved more than a 5-fold increase in hydroxycineole production using fusion proteins *in vitro* and 3-fold *in vivo* over the control using individual enzymes. Structural characterization of these enzyme fusions revealed that the length of the linker affects the flexibility, which eventually affects the catalytic activity, of the fusion enzymes. We also applied the enzyme fusion strategy to the oxidation of a sesquiterpene epi-isozizaene, in which up to 90-fold improvement in albaflavenol production was achieved by the fusion enzyme when the overlay was used. Our results suggested that engineering of fusion enzymes between terpene synthase and P450 shows a simple and efficient strategy toward the heterologous production of oxidized terpenes. Additionally, the structure-based prediction and evaluation would guide the design of fusion proteins with improved catalysis.

Acknowledgments

This work was part of the DOE Joint BioEnergy Institute (http://www.jbei.org) supported by the US Department of Energy, Office of Science, Office of Biological and Environmental Research, through Contract DE-AC0205CH11231 between Lawrence Berkeley National Laboratory and the US Department of Energy. SAXS data was collected at the SIBYLS beamline in the Advanced Light Source, which is supported by DOE BES, by the DOE OBER IDAT program, by NIH ALS-ENABLE (P30 GM124169) and by NIH S10OD018483. We would also like to acknowledge the help of beamline staff, Daniel Rosenberg and Michal Hammel.

Author contributions

XW and TSL designed the experiments. XW performed the experiments and structural modeling. JHP and ST performed the SAXS experiment. XW, TSL, JHP, and ST analyzed the data, wrote the manuscript. All authors reviewed and edited the final manuscript.

Competing interests

TSL has a financial interest in Maple Bio.

References

Aaron, J.A., Lin, X., Cane, D.E., Christianson, D.W., 2010. Structure of epi-isozizaene synthase from *Streptomyces coelicolor* A3(2), a platform for new terpenoid cyclization templates,. Biochemistry 49, 1787–1797.

Aharoni, A., Jongsma, M.A., Bouwmeester, H.J., 2005. Volatile science? Metabolic engineering of terpenoids in plants. Trends Plant Sci. 10, 594–602.

Alonso-Gutierrez, J., Chan, R., Batth, T.S., Adams, P.D., Keasling, J.D., Petzold, C.J., Lee, T.S., 2013. Metabolic engineering of Escherichia coli for limonene and perillyl alcohol production. Metab. Eng. 19, 33–41.

Avalos, J.L., Fink, G.R., Stephanopoulos, G., 2013. Compartmentalization of metabolic pathways in yeast mitochondria improves the production of branched-chain alcohols. Nat. Biotechnol. 31, 335.

Bakkes, P.J., Biemann, S., Bokel, A., Eickholt, M., Girhard, M., Urlacher, V.B., 2015. Design and improvement of artificial redox modules by molecular fusion of flavodoxin and flavodoxin reductase from *Escherichia coli*. Sci. Rep. 5, 12158.

Bakkes, P.J., Riehm, J.L., Sagadin, T., Rühlmann, A., Schubert, P., Biemann, S., Girhard, M.,

Hutter, M.C., Bernhardt, R., Urlacher, V.B., 2017. Engineering of versatile redox partner fusions that support monooxygenase activity of functionally diverse cytochrome P450s. Sci. Rep. 7, 9570.

Belsare, K.D., Ruff, A.J., Martinez, R., Shivange, A. V, Mundhada, H., Holtmann, D., Schrader, J., Schwaneberg, U., 2014. P-LinK: A method for generating multicomponent cytochrome P450 fusions with variable linker length. Biotechniques 57, 13–20.

Bergman, A., Siewers, V., 2016. Chapter 7 - Metabolic engineering strategies to convert carbohydrates to aviation range hydrocarbons, in: Chuck, C.J.B.T.-B. for A. (Ed.), . Academic Press, pp. 151–190.

Bernhardt, R., 2006. Cytochromes P450 as versatile biocatalysts. J. Biotechnol. 124, 128–145.

Brosey, C.A., Yan, C., Tsutakawa, S.E., Heller, W.T., Rambo, R.P., Tainer, J.A., Ivanov, I., Chazin, W.J., 2013. A new structural framework for integrating replication protein A into DNA processing machinery. Nucleic Acids Res. 41, 2313–2327.

Chang, M.C.Y., Eachus, R.A., Trieu, W., Ro, D.-K., Keasling, J.D., 2007. Engineering Escherichia coli for production of functionalized terpenoids using plant P450s. Nat. Chem. Biol. 3, 274.

Cheng, A.-X., Lou, Y.-G., Mao, Y.-B., Lu, S., Wang, L.-J., Chen, X.-Y., 2007. Plant terpenoids: biosynthesis and ecological functions. J. Integr. Plant Biol. 49, 179–186.

Classen, S., Hura, G.L., Holton, J.M., Rambo, R.P., Rodic, I., McGuire, P.J., Dyer, K., Hammel, M., Meigs, G., Frankel, K.A., Tainer, J.A., 2013. Implementation and performance of SIBYLS: a dual endstation small-angle X-ray scattering and macromolecular crystallography beamline at the Advanced Light Source. J. Appl. Crystallogr. 46, 1–13.

Conrado, R.J., Varner, J.D., DeLisa, M.P., 2008. Engineering the spatial organization of

metabolic enzymes: mimicking nature’s synergy. Curr. Opin. Biotechnol. 19, 492–499.

Crasto, C.J., Feng, J., 2000. LINKER: a program to generate linker sequences for fusion proteins. Protein Eng. Des. Sel. 13, 309–312.

Dueber, J.E., Wu, G.C., Malmirchegini, G.R., Moon, T.S., Petzold, C.J., Ullal, A. V, Prather, K.L.J., Keasling, J.D., 2009. Synthetic protein scaffolds provide modular control over metabolic flux. Nat. Biotechnol. 27, 753–759.

Dyer, K.N., Hammel, M., Rambo, R.P., Tsutakawa, S.E., Rodic, I., Classen, S., Tainer, J.A., Hura, G.L., 2014. High-Throughput SAXS for the Characterization of Biomolecules in Solution: A Practical Approach, in: Chen, Y.W. (Ed.), Structural Genomics: General Applications. Humana Press, Totowa, NJ, pp. 245–258.

Fiser, A., Do, R.K.G., Šali, A., 2000. Modeling of loops in protein structures. Protein Sci. 9, 1753–1773.

Franke, D., Petoukhov, M. V, Konarev, P. V, Panjkovich, A., Tuukkanen, A., Mertens, H.D.T., Kikhney, A.G., Hajizadeh, N.R., Franklin, J.M., Jeffries, C.M., Svergun, D.I., 2017. {\it ATSAS 2.8}: a comprehensive data analysis suite for small-angle scattering from macromolecular solutions. J. Appl. Crystallogr. 50, 1212–1225.

Gao, X., Gao, F., Liu, D., Zhang, H., Nie, X., Yang, C., 2016. Engineering the methylerythritol phosphate pathway in cyanobacteria for photosynthetic isoprene production from CO2. Energy Environ. Sci. 9, 1400–1411.

Guo, H., Yang, Y., Xue, F., Zhang, H., Huang, T., Liu, W., Liu, H., Zhang, F., Yang, M., Liu, C., Lu, H., Zhang, Y., Ma, L., 2017. Effect of flexible linker length on the activity of fusion protein 4-coumaroyl-CoA ligase::stilbene synthase. Mol. Biosyst. 13, 598–606.

Haudenschild, C., Schalk M FAU - Karp, F., Karp F FAU - Croteau, R., Croteau, R., 2000.

591 Functional expression of regiospecific cytochrome P450 limonene hydroxylases from mint
592 (Mentha spp.) in Escherichia coli and saccharomyces cerevisiae. Archi. Biochem. Biophys.
593 379, 127–136.
594 Hawkes, D.B., Adams, G.W., Burlingame, A.L., Ortiz de Montellano, P.R., De Voss, J.J., 2002.
595 Cytochrome P450cin (CYP176A), isolation, expression, and characterization . J. Biol.
596 Chem. 277, 27725–27732.
597 Hawkes, D.B., Slessor, K.E., Bernhardt, P. V, De Voss, J.J., 2010. Cloning, expression and
598 purification of cindoxin, an unusual Fmn-containing cytochrome P450 redox partner.
599 ChemBioChem 11, 1107–1114.
600 Hoffmann, S.M., Weissenborn, M.J., Gricman, Ł., Notonier, S., Pleiss, J., Hauer, B., 2016. The
601 impact of linker length on P450 fusion constructs: activity, stability and coupling.
602 ChemCatChem 8, 1591–1597.
603 Hura, G.L., Menon, A.L., Hammel, M., Rambo, R.P., Poole II, F.L., Tsutakawa, S.E., Jenney Jr,
604 F.E., Classen, S., Frankel, K.A., Hopkins, R.C., Yang, S., Scott, J.W., Dillard, B.D., Adams,
605 M.W.W., Tainer, J.A., 2009. Robust, high-throughput solution structural analyses by small
606 angle X-ray scattering (SAXS). Nat. Methods 6, 606–612.
607 Hyatt, D.C., Youn, B., Zhao, Y., Santhamma, B., Coates, R.M., Croteau, R.B., Kang, C., 2007.
608 Structure of limonene synthase, a simple model for terpenoid cyclase catalysis. Proc. Natl.
609 Acad. Sci. 104, 5360 LP – 5365.
610 Jenkins, C.M., Waterman, M.R., 1994. Flavodoxin and NADPH-flavodoxin reductase from
611 *Escherichia coli* support bovine cytochrome P450c17 hydroxylase activities. J. Biol. Chem.
612 269, 27401–27408.
613 Kang, A., George, K.W., Wang, G., Baidoo, E., Keasling, J.D., Lee, T.S., 2016. Isopentenyl

614 diphosphate (IPP)-bypass mevalonate pathways for isopentenol production. Metab. Eng. 34,
615 25–35.
616 Karuppiah, V., Ranaghan, K.E., Leferink, N.G.H., Johannissen, L.O., Shanmugam, M., Ní
617 Cheallaigh, A., Bennett, N.J., Kearsey, L.J., Takano, E., Gardiner, J.M., van der Kamp,
618 M.W., Hay, S., Mulholland, A.J., Leys, D., Scrutton, N.S., 2017. Structural basis of
619 catalysis in the bacterial monoterpene synthases linalool synthase and 1,8-cineole synthase.
620 ACS Catal. 7, 6268–6282.
621 Khatri, Y., Schifrin, A., Bernhardt, R., 2017. Investigating the effect of available redox protein
622 ratios for the conversion of a steroid by a myxobacterial CYP260A1. FEBS Lett. 591,
623 1126–1140.
624 Kimmich, N., Das, A., Sevrioukova, I., Meharenna, Y., Sligar, S.G., Poulos, T.L., 2007. Electron
625 Transfer between Cytochrome P450cin and Its FMN-containing Redox Partner, Cindoxin. J.
626 Biol. Chem. 282, 27006–27011.
627 Klocke, J.A., Darlington, M. V, Balandrin, M.F., 1987. 1,8-Cineole (Eucalyptol), a mosquito
628 feeding and ovipositional repellent from volatile oil ofHemizonia fitchii (Asteraceae). J.
629 Chem. Ecol. 13, 2131–2141.
630 Kourtz, L., Dillon, K., Daughtry, S., Madison, L.L., Peoples, O., Snell, K.D., 2005. A novel
631 thiolase–reductase gene fusion promotes the production of polyhydroxybutyrate in
632 Arabidopsis. Plant Biotechnol. J. 3, 435–447.
633 Leita, B.A., Warden, A.C., Burke, N., O'Shea, M.S., Trimm, D., 2010. Production of p-cymene
634 and hydrogen from a bio-renewable feedstock–1,8-cineole (eucalyptus oil). Green Chem.
635 12, 70–76.
636 Li, S., Du, L., Bernhardt, R., 2020. Redox Partners: Function Modulators of Bacterial P450

637 Enzymes. Trends Microbiol. 28, 445–454.
638 Liu, C.-L., Tian, T., Alonso-Gutierrez, J., Garabedian, B., Wang, S., Baidoo, E.E.K., Benites, V.,
639 Chen, Y., Petzold, C.J., Adams, P.D., Keasling, J.D., Tan, T., Lee, T.S., 2018. Renewable
640 production of high density jet fuel precursor sesquiterpenes from Escherichia coli.
641 Biotechnol. Biofuels 11, 285.
642 Liu, C., Chin, J.X., Lee, D.-Y., 2015. SynLinker: an integrated system for designing linkers and
643 synthetic fusion proteins. Bioinformatics 31, 3700–3702.
644 Ljungcrantz, P., Carlsson, H., Mansson, M.O., Buckel, P., Mosbach, K., Buelow, L., 1989.
645 Construction of an artificial bifunctional enzyme, .beta.-galactosidase/galactose
646 dehydrogenase, exhibiting efficient galactose channeling. Biochemistry 28, 8786–8792.
647 Madrona, Y., Hollingsworth, S.A., Tripathi, S., Fields, J.B., Rwigema, J.-C.N., Tobias, D.J.,
648 Poulos, T.L., 2014. Crystal structure of cindoxin, the P450cin redox partner. Biochemistry
649 53, 1435–1446.
650 Meharenna, Y.T., Li, H., Hawkes, D.B., Pearson, A.G., De Voss, J., Poulos, T.L., 2004. Crystal
651 structure of P450cin in a complex with its substrate, 1,8-cineole, a close structural
652 homologue to d-camphor, the substrate for P450cam,. Biochemistry 43, 9487–9494.
653 Mendez-Perez, D., Alonso-Gutierrez, J., Hu, Q., Molinas, M., Baidoo, E.E.K., Wang, G., Chan,
654 L.J.G., Adams, P.D., Petzold, C.J., Keasling, J.D., Lee, T.S., 2017. Production of jet fuel
655 precursor monoterpenoids from engineered *Escherichia coli*. Biotechnol. Bioeng. 114,
656 1703–1712.
657 Meynial Salles, I., Forchhammer, N., Croux, C., Girbal, L., Soucaille, P., 2007. Evolution of a
658 *Saccharomyces cerevisiae* metabolic pathway in *Escherichia coli*. Metab. Eng. 9, 152–159.
659 Moser, S., Pichler, H., 2019. Identifying and engineering the ideal microbial terpenoid

660 production host. Appl. Microbiol. Biotechnol. 103, 5501–5516.
661 Pateraki, I., Heskes, A.M., Hamberger, B., 2015. Cytochromes P450 for terpene functionalisation
662 and metabolic engineering BT - biotechnology of isoprenoids, in: Schrader, J., Bohlmann,
663 J. (Eds.), . Springer International Publishing, Cham, pp. 107–139.
664 Pelikan, M., Hura, G.L., Hammel, M., 2009. Structure and flexibility within proteins as
665 identified through small angle X-ray scattering. Gen. Physiol. Biophys. 28, 174–189.
666 Pham, S.Q., Pompidor, G., Liu, J., Li, X.-D., Li, Z., 2012. Evolving P450pyr hydroxylase for
667 highly enantioselective hydroxylation at non-activated carbon atom. Chem. Commun. 48,
668 4618–4620.
669 Putnam, C.D., Hammel, M., Hura, G.L., Tainer, J.A., 2007. X-ray solution scattering (SAXS)
670 combined with crystallography and computation: defining accurate macromolecular
671 structures, conformations and assemblies in solution. Q. Rev. Biophys. 40, 191–285.
672 Rambo, R.P., Tainer, J.A., 2013. Accurate assessment of mass, models and resolution by small-
673 angle scattering. Nature 496, 477–481.
674 Rambo, R.P., Tainer, J.A., 2011. Characterizing flexible and intrinsically unstructured biological
675 macromolecules by SAS using the Porod-Debye law. Biopolymers 95, 559–571.
676 Redding-Johanson, A.M., Batth, T.S., Chan, R., Krupa, R., Szmidt, H.L., Adams, P.D., Keasling,
677 J.D., Soon Lee, T., Mukhopadhyay, A., Petzold, C.J., 2011. Targeted proteomics for
678 metabolic pathway optimization: Application to terpene production. Metab. Eng. 13, 194–
679 203.
680 Renault, H., Bassard, J.-E., Hamberger, B., Werck-Reichhart, D., 2014. Cytochrome P450-
681 mediated metabolic engineering: current progress and future challenges. Curr. Opin. Plant
682 Biol. 19, 27–34.

683 Roy, A., Yang, J., Zhang, Y., 2012. COFACTOR: an accurate comparative algorithm for
684 structure-based protein function annotation. Nucleic Acids Res. 40, W471–W477.
685 Sarria, S., Wong, B., Martín, H.G., Keasling, J.D., Peralta-Yahya, P., 2014. Microbial synthesis
686 of pinene. ACS Synth. Biol. 3, 466–475.
687 Schiffer, L., Anderko, S., Hobler, A., Hannemann, F., Kagawa, N., Bernhardt, R., 2015. A
688 recombinant CYP11B1 dependent Escherichia coli biocatalyst for selective cortisol
689 production and optimization towards a preparative scale. Microb. Cell Fact. 14, 25.
690 Schneidman-Duhovny, D., Hammel, M., Tainer, J.A., Sali, A., 2016. FoXS, FoXSDock and
691 MultiFoXS: Single-state and multi-state structural modeling of proteins and their complexes
692 based on SAXS profiles. Nucleic Acids Res. 44, W424–W429.
693 Schneidman-Duhovny, D., Hammel, M., Tainer, J.A., Sali, A., 2013. Accurate SAXS profile
694 computation and its assessment by contrast variation experiments. Biophys. J. 105, 962–
695 974.
696 Shaw, J.J., Berbasova, T., Sasaki, T., Jefferson-George, K., Spakowicz, D.J., Dunican, B.F.,
697 Portero, C.E., Narváez-Trujillo, A., Strobel, S.A., 2015. Identification of a fungal 1,8-
698 cineole synthase from hypoxylon sp. with specificity determinants in common with the
699 plant synthases . J. Biol. Chem. 290, 8511–8526.
700 Slessor, K.E., Hawkes, D.B., Farlow, A., Pearson, A.G., Stok, J.E., De Voss, J.J., 2012. An in
701 vivo cytochrome P450cin (CYP176A1) catalytic system for metabolite production. J. Mol.
702 Catal. B Enzym. 79, 15–20.
703 Urlacher, V.B., Girhard, M., 2019. Cytochrome P450 monooxygenases in biotechnology and
704 synthetic biology. Trends Biotechnol. 37, 882–897.
705 van Beilen, J.B., Holtackers, R., Lüscher, D., Bauer, U., Witholt, B., Duetz, W.A., 2005.

Biocatalytic production of perillyl alcohol from limonene by using a novel *Mycobacterium* sp. cytochrome P450 alkane hydroxylase expressed in *Pseudomonas putida*. Appl. Environ. Microbiol. 71, 1737 LP – 1744.

Williams, D.C., McGarvey, D.J., Katahira, E.J., Croteau, R., 1998. Truncation of limonene synthase preprotein provides a fully active 'pseudomature' form of this monoterpene cyclase and reveals the function of the amino-terminal arginine pair. Biochemistry 37, 12213–12220.

Yang, J., Zhang, Y., 2015. I-TASSER server: new development for protein structure and function predictions. Nucleic Acids Res. 43, W174–W181.

Yang, X., Li, T., Tang, K., Zhou, X., Lu, M., Ounkham, W.L., Spain, S.M., Frost, B.J., Lin, H., 2017. Highly efficient conversion of terpenoid biomass to jet-fuel range cycloalkanes in a biphasic tandem catalytic process. Green Chem. 19, 3566–3573.

Yu, K., Liu, C., Kim, B.-G., Lee, D.-Y., 2015. Synthetic fusion protein design and applications. Biotechnol. Adv. 33, 155–164.

Zhang, Y., 2009. I-TASSER: Fully automated protein structure prediction in CASP8. Proteins Struct. Funct. Bioinforma. 77, 100–113.

Zhao, B., Lei, L., Vassylyev, D.G., Lin, X., Cane, D.E., Kelly, S.L., Yuan, H., Lamb, D.C., Waterman, M.R., 2009. Crystal structure of albaflavenone monooxygenase containing a moonlighting terpene synthase active site. J. Biol. Chem. 284, 36711–36719.

Zhao, B., Lin, X., Lei, L., Lamb, D.C., Kelly, S.L., Waterman, M.R., Cane, D.E., 2008. Biosynthesis of the sesquiterpene antibiotic albaflavenone in *Streptomyces coelicolor* A3(2). J. Biol. Chem. 283, 8183–8189.

Zuo, R., Zhang, Y., Jiang, C., Hackett, J.C., Loria, R., Bruner, S.D., Ding, Y., 2017. Engineered

729 P450 biocatalysts show improved activity and regio-promiscuity in aromatic nitration. Sci.
730 Rep. 7, 842.
731

732 **Table 1** Strains and plasmids used in this study

Strains	**Description**	**Reference**
CS	*E. coli* BL21 (DE3) with pSKB3-CS	This study
CinA	*E. coli* BL21 (DE3) with pSKB3-CinA	This study
CinC	*E. coli* BL21 (DE3) with pSKB3-CinC	This study
G1	*E. coli* BL21 (DE3) with pSKB3-CS-$(GSG)_1$-CinA	This study
G2	*E. coli* BL21 (DE3) with pSKB3-CS-$(GSG)_2$-CinA	This study
G3	*E. coli* BL21 (DE3) with pSKB3-CS-$(GSG)_3$-CinA	This study
G4	*E. coli* BL21 (DE3) with pSKB3-CS-$(GSG)_4$-CinA	This study
G5	*E. coli* BL21 (DE3) with pSKB3-CS-$(GSG)_5$-CinA	This study
Fpr	*E. coli* BL21 (DE3) with pSKB3-Fpr	This study
2pCin_Non-fusion	*E. coli* DH1 with JBEI-3122 + pTrc99a-trGPPS-CS-RBS-CinA-CinC	This study
CS-$(GSG)_1$-$P450_{cin}$	*E. coli* DH1 with JBEI-3122 + pTrc99a-trGPPS-CS-$(GSG)_1$-CinA-CinC	This study
CS-$(GSG)_2$-$P450_{cin}$	*E. coli* DH1 with JBEI-3122 + pTrc99a-trGPPS-CS-$(GSG)_2$-CinA-CinC	This study
CS-$(GSG)_3$-$P450_{cin}$	*E. coli* DH1 with JBEI-3122 + pTrc99a-trGPPS-CS-$(GSG)_3$-CinA-CinC	This study
CS-$(GSG)_4$-$P450_{cin}$	*E. coli* DH1 with JBEI-3122 + pTrc99a-trGPPS-CS-$(GSG)_4$-CinA-CinC	This study
CS-$(GSG)_5$-$P450_{cin}$	*E. coli* DH1 with JBEI-3122 + pTrc99a-trGPPS-CS-$(GSG)_5$-CinA-CinC	This study
$P450_{cin}$-$(GSG)_3$-CS	*E. coli* DH1 with JBEI-3122 + pTrc99a-trGPPS-CinA-$(GSG)_3$-CS-CinC	This study
2pEiz	*E. coli* DH1 with JBEI-2704 + JBEI-15862	This study
2pEiz_Non-fusion	*E. coli* DH1 with JBEI-2704 + pTrc99a-EizS-RBS-CYP170A1-CinC	This study
EizS-$(GSG)_1$-CYP170A1	*E. coli* DH1 with JBEI-2704 + pTrc99a-EizS-$(GSG)_1$-CYP170A1-CinC	This study
EizS-$(GSG)_2$-CYP170A1	*E. coli* DH1 with JBEI-2704 + pTrc99a-EizS-$(GSG)_2$-CYP170A1-CinC	This study
EizS-$(GSG)_3$-CYP170A1	*E. coli* DH1 with JBEI-2704 + pTrc99a-EizS-$(GSG)_3$-CYP170A1-CinC	This study
EizS-$(GSG)_4$-CYP170A1	*E. coli* DH1 with JBEI-2704 + pTrc99a-EizS-$(GSG)_4$-CYP170A1-CinC	This study
EizS-$(GSG)_5$-CYP170A1	*E. coli* DH1 with JBEI-2704 + pTrc99a-EizS-$(GSG)_5$-CYP170A1-CinC	This study
Plasmids	**Description**	**Reference**

pSKB3	Modified pET-28a	(Kang et al., 2016)
JBEI-3122	pBbA5c-MTSA-T1-MBI	(Alonso-Gutierrez et al., 2013)
JBEI-15065	pTrc99a-GPPS-CS_{Str}	(Mendez-Perez et al., 2017)
JBEI-2704	pBbA5c-MevT-T1-MBIS	(Redding-Johanson et al., 2011)
JBEI-15862	pTrc99a-coEizS	(Liu et al., 2018)
JPUB_016968	pSKB3-CS	This study
JPUB_016970	pSKB3-CinA	This study
JPUB_016972	pSKB3-CinC	This study
JPUB_016974	pSKB3-CS-G1-CinA	This study
JPUB_016976	pSKB3-CS-G2-CinA	This study
JPUB_016978	pSKB3-CS-G3-CinA	This study
JPUB_016980	pSKB3-CS-G4-CinA	This study
JPUB_016982	pSKB3-CS-G5-CinA	This study
JPUB_016984	pSKB3-Fpr	This study
JPUB_016986	pTrc99a-trGPPS-CS-RBS-CinA-CinC	This study
JPUB_016988	pTrc99a-trGPPS-CS-$(GSG)_1$-CinA-CinC	This study
JPUB_016990	pTrc99a-trGPPS-CS-$(GSG)_2$-CinA-CinC	This study
JPUB_016992	pTrc99a-trGPPS-CS-$(GSG)_3$-CinA-CinC	This study
JPUB_016994	pTrc99a-trGPPS-CS-$(GSG)_4$-CinA-CinC	This study
JPUB_016996	pTrc99a-trGPPS-CS-$(GSG)_5$-CinA-CinC	This study
JPUB_016998	pTrc99a-trGPPS-CinA-$(GSG)_3$-CS-CinC	This study
JPUB_017000	pTrc99a-EizS-RBS-CYP170A1-CinC	This study
JPUB_017002	pTrc99a-EizS-$(GSG)_1$-CYP170A1-CinC	This study
JPUB_017003	pTrc99a-EizS-$(GSG)_2$-CYP170A1-CinC	This study
JPUB_017005	pTrc99a-EizS-$(GSG)_3$-CYP170A1-CinC	This study
JPUB_017007	pTrc99a-EizS-$(GSG)_4$-CYP170A1-CinC	This study
JPUB_017009	pTrc99a-EizS-$(GSG)_5$-CYP170A1-CinC	This study

733

Table 2 SAXS Data collection and metrics

SEC-SAXS Data	G3 monomer	G3 dimer	G4 monomer	G4 dimer
Nomenclature	222	221	232	231
Porod Debye (Px)	3.9	3.4	3.3	3.3
Low q ($Å^{-1}$)	0.0137	0.0158	0.0209	0.0137
High q ($Å^{-1}$)	0.366	0.366	0.366	0.366
Reciprocal Rg (Å)	33	44	36	46
Reciprocal I(0) (detector units)	111	191	374	2,940
Real space Rg (Å)	33	44	35	46
Real space I(0) (detector units)	111	191	374	2,940
Dmax (Å)	96	150	106	158
Vc Molecular Mass (kDa)	85	147	85	153
Theoretical Mass (kDa) [dimer]	86.6	[173]	86.7	[173]

Table 3 Characterization of the fusion protein with the reversed orientation of enzymes ($P450_{cin}$-CS) during the *in vivo* hydroxycineole production

	1,8-Cineole (mg/L)		**Hydroxycineole (mg/L)** *	
	With overlay	Without overlay	With overlay	Without overlay
Non-fusion	88 ± 14	2 ± 0	10 ± 0	18 ± 1
CS-$P450_{cin}$	86 ± 1	3 ± 1	32 ± 1	56 ± 1
$P450_{cin}$-CS	42 ± 10	1 ± 0	8 ± 0	21 ± 1

Data are represented as mean ± standard deviation of triplicates.

***** Hydroxycineole concentrations are reported based on the equivalent concentration of 1,8-cineole.

Figures

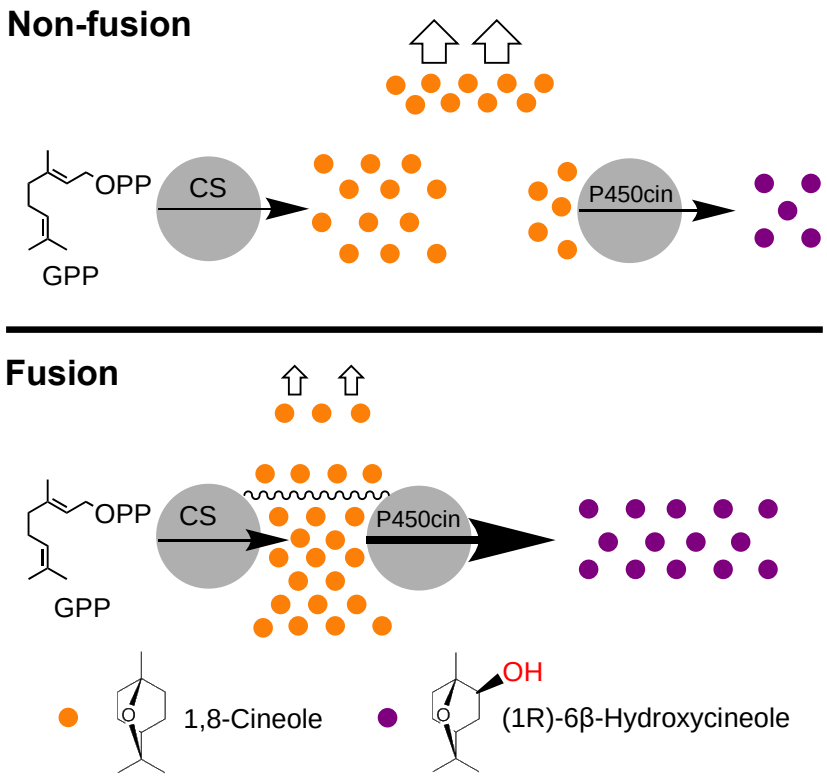

Graphical abstract

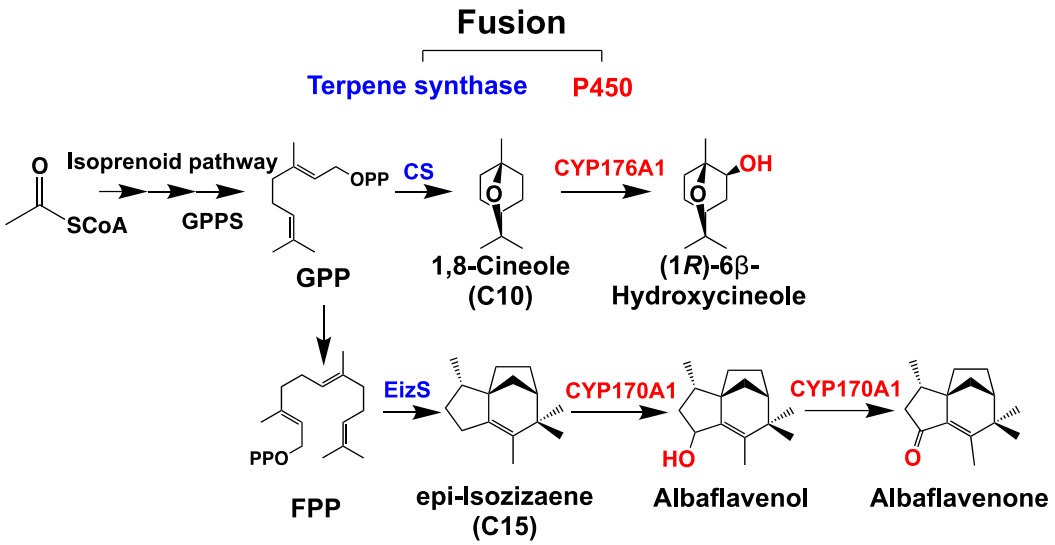

765

766 **Figure 1** Engineering enzyme fusions by linking terpene synthase (CS, EizS) and P450 enzyme

767 (CYP) for the production of oxidized terpenoids. GPP, geranyl pyrophosphate; FPP, farnesyl

768 pyrophosphate; CS, 1,8-cineole synthase; EizS, epi-isozizaene synthase; GPPS, geranyl

769 pyrophosphate synthase.

770

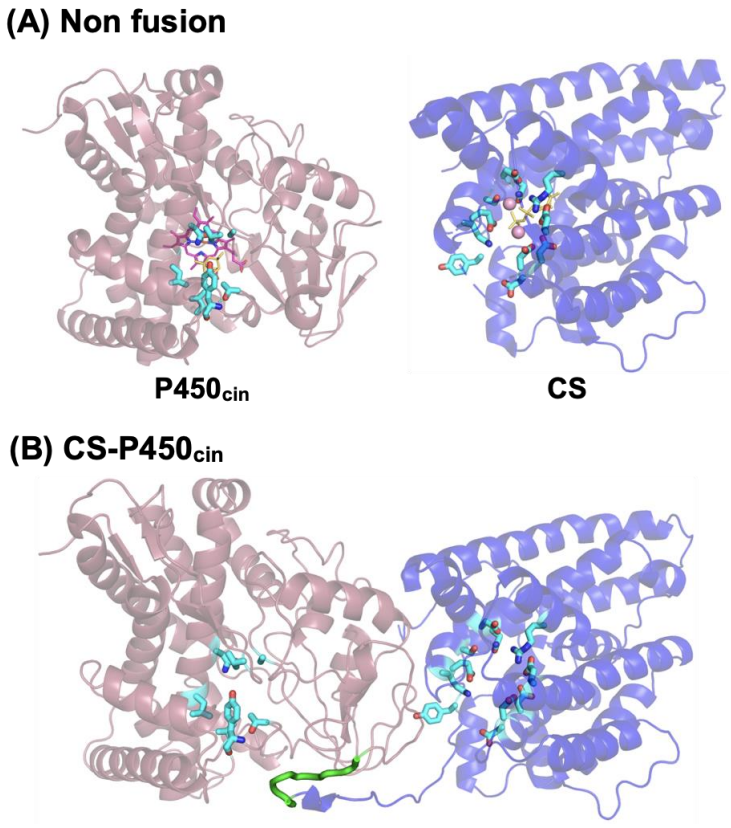

771

772 **Figure 2** Structural prediction of CS-$P450_{cin}$ fusion protein. (A) Structures of non-fused enzymes

773 of $P450_{cin}$ and CS monomer aligned with the predicted structure of CS-$P450_{cin}$ fusion. (B)

774 Predicted structure of the CS-$P450_{cin}$ fusion protein with a $(GSG)_3$ peptide linker (G3), C-score

775 of I-TASSER = -2.74. $P450_{cin}$, red cartoon; CS, blue cartoon; $(GSG)_3$ linker, green loop; Heme,

776 pink stick molecule; Residues of active sites, color stick molecules.

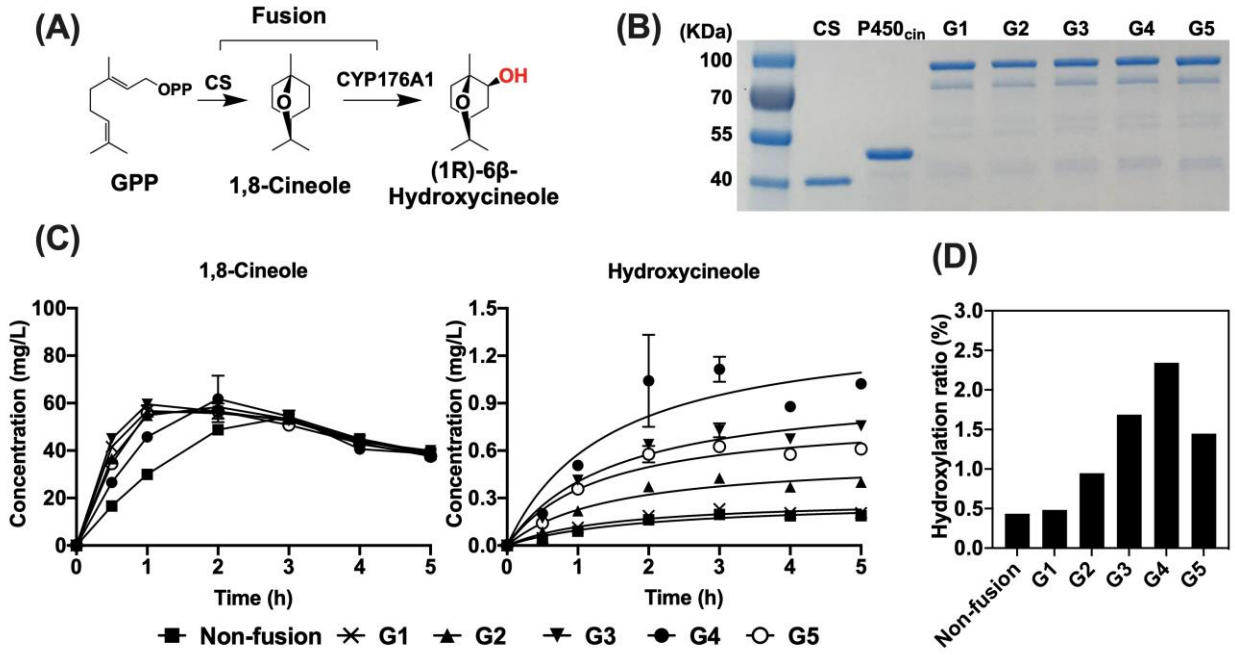

Figure 3 *In vitro* production of hydroxycineole. (A) *In vitro* two-step reaction from GPP. (B) SDS-PAGE gel of purified non-fusion and fusions for CS and $P450_{cin}$. Fusions of CS and $P450_{cin}$ (G1 to G5) were engineered with 1 to 5 repeats of GSG peptide linker. Size of purified proteins: CS, 40.71 KDa; $P450_{cin}$ (CinA), 48.25 KDa; G1, 86.16 KDa; G2, 86.37 KDa; G3, 86.57 KDa; G4, 86.77 KDa; G5, 86.97 KDa. (C) *In vitro* time-course production of cineole and hydroxycineole from GPP substrate with purified proteins. Hydroxycineole concentrations are reported based on the equivalent concentration of 1,8-cineole. Error bars indicate one standard deviation (n = 3). (D) Hydroxylation ratio of *in vitro* reaction after 5 hours. The hydroxylation ratio is the molar ratio of hydroxycineole out of the total generated terpenes (1,8-cineole and hydroxycineole).

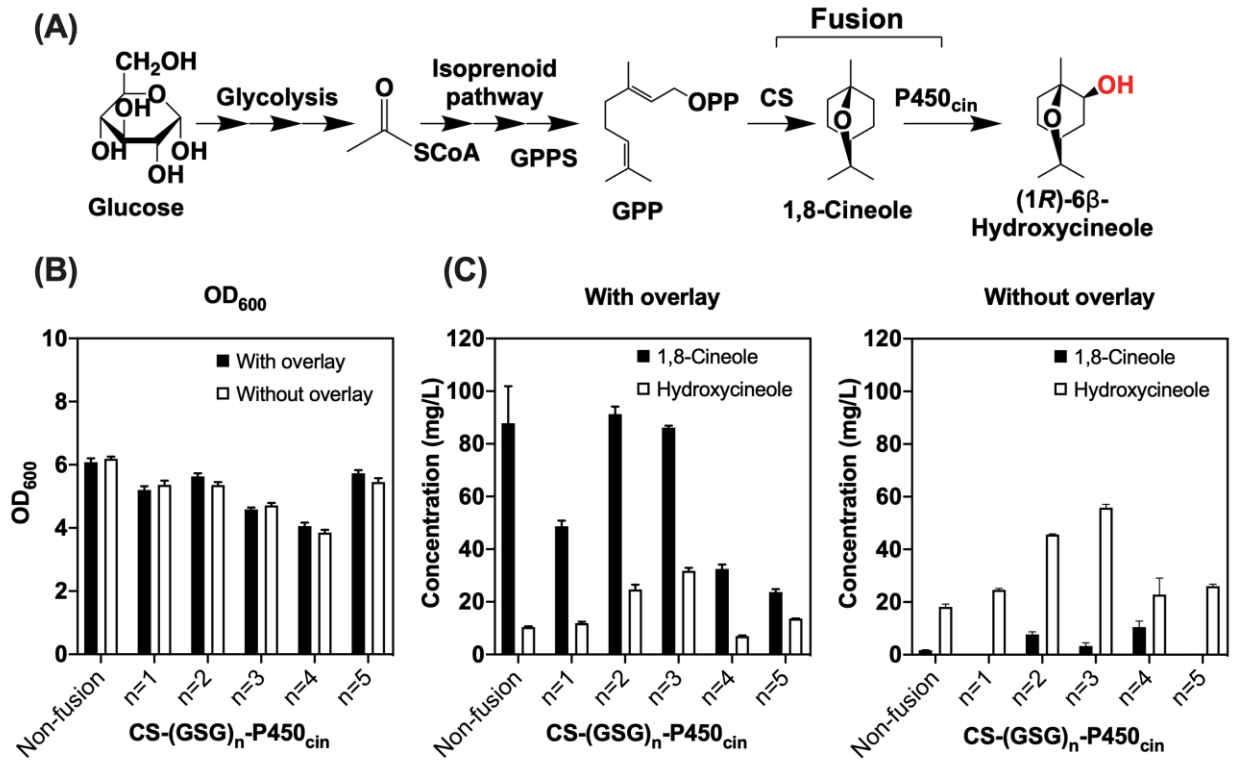

789

790 **Figure 4** *In vivo* production of hydroxycineole by *E. coli* DH1 strains with engineered enzyme

791 fusions. (A) Metabolic pathway of hydroxycineole production from glucose using enzyme

792 fusions of CS and $P450_{cin}$, CS-$(GSG)_n$-$P450_{cin}$ (n = 1–5). (B) OD_{600} of production strains after 48

793 hours. (C) Production of 1,8-cineole and hydroxycineole with or without the solvent overlay.

794 Hydroxycineole concentrations are reported based on the equivalent concentration of 1,8-cineole.

795 Error bars indicate one standard deviation of triplicates.

796

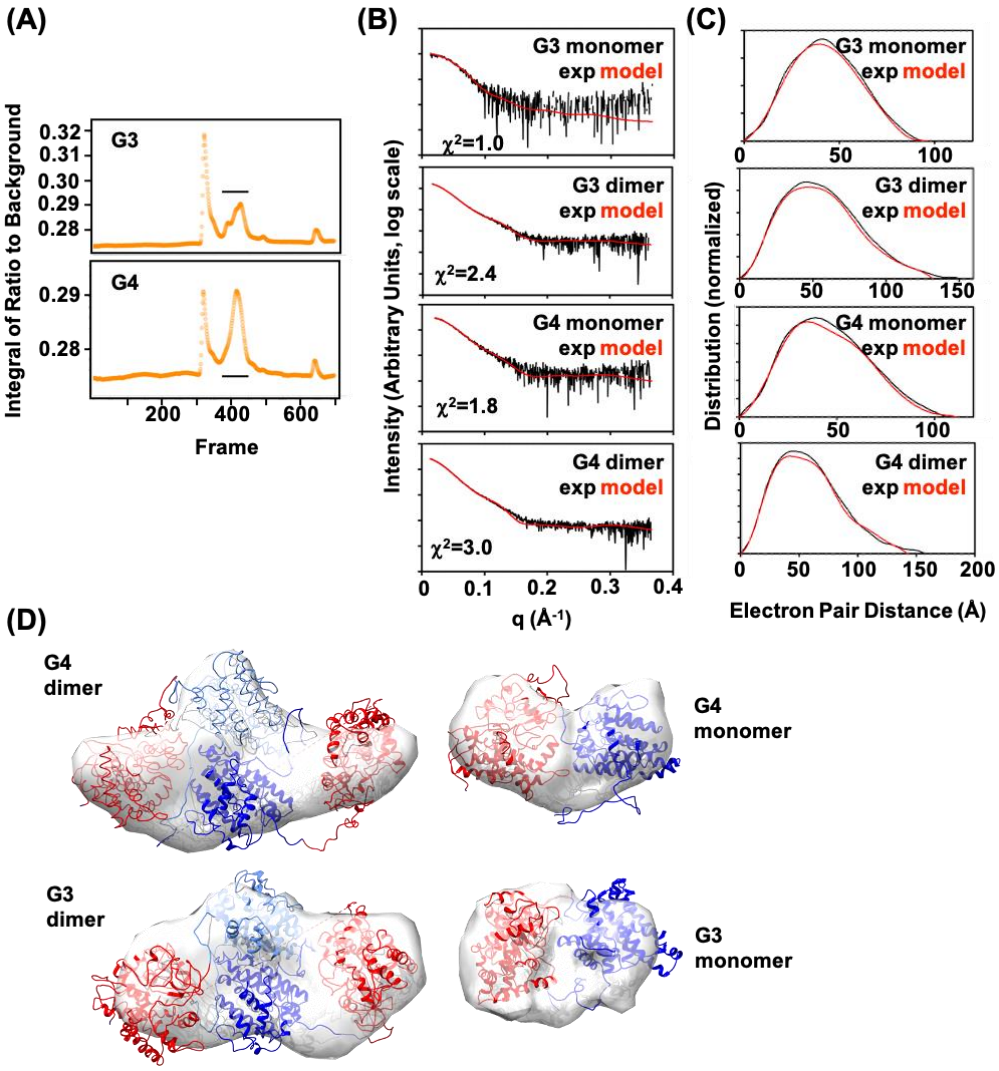

Figure 5 SAXS analysis of enzyme fusions. (A) SEC-SAXS chromatogram of G3 and G4 fusion proteins. The horizontal line indicates peak(s) that were further analyzed. (B) Reciprocal space SAXS curves after SVD, representing scattering from monomer and dimer for G3 and G4 enzyme fusions, overlaid with curves predicted from models that best fit the experimental data (red curves). χ^2 fit of models is shown. (C) Corresponding real space SAXS curves with experimental and model curves overlaid. (D) Ab initio shape predictions overlaid with the best-fitting model. Models were based on 1,8-cineole synthase (PDB ID: 5NX6, blue) and $P450_{cin}$ (PDB ID:1T2B, red).

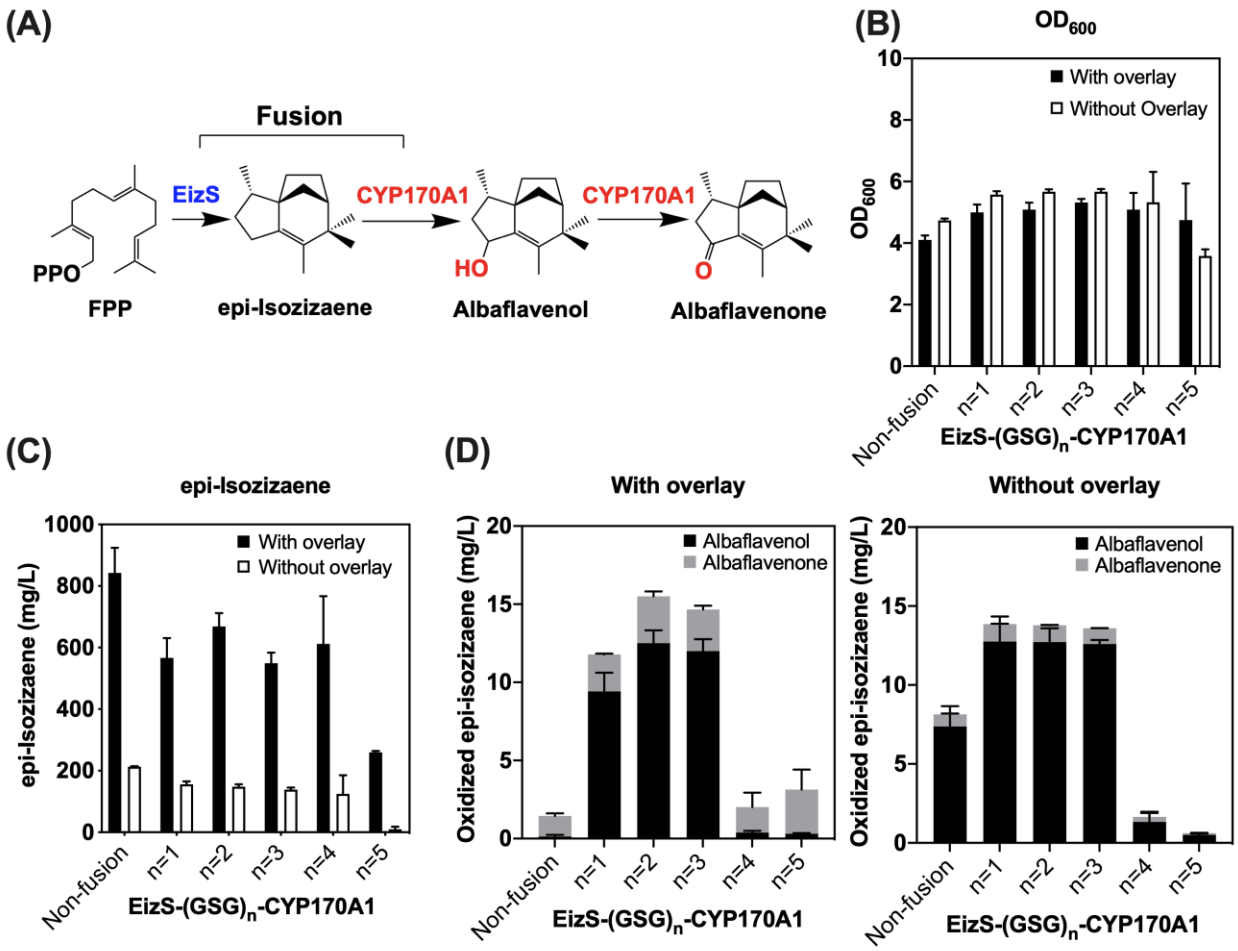

806

807 **Figure 6** Production of oxidized epi-isozizaene with engineered enzyme fusions in *E. coli* DH1.

808 (A) Metabolic pathway of oxidized epi-isozizaene production from glucose using enzyme

809 fusions of EizS and CYP170A1, EizS-$(GSG)_n$-CYP170A1 (n = 1–5); FPP, farnesyl

810 pyrophosphate. (B) OD_{600} of production strains after 72 hours. (C) Production of epi-isozizaene

811 with or without the solvent overlay. (D) Production of oxidized epi-isozizaene (albaflavenol,

812 albaflavenone) with or without the solvent overlay. The concentrations of epi-isozizaene,

813 albaflavenol, and albaflavenone are reported based on the equivalent concentration of (-)-trans

814 caryophyllene. Error bars indicate one standard deviation of triplicates.